Published in Current Biology 24(15): 1679–1688, 2014
which should be cited to refer to this work

Activity-Dependent Structural Plasticity of Perisynaptic Astrocytic Domains Promotes Excitatory Synapse Stability

Yann Bernardinelli,[1,*] Jerome Randall,[1] Elia Janett,[2] Irina Nikonenko,[1] Stéphane König,[1] Emma Victoria Jones,[3] Carmen E. Flores,[1] Keith K. Murai,[3] Christian G. Bochet,[2] Anthony Holtmaat,[1] and Dominique Muller[1]

[1]Department of Basic Neurosciences, Medical School, University of Geneva, Rue Michel-Servet 1, 1211 Geneva 4, Switzerland

[2]Department of Chemistry, University of Fribourg, Chemin du Musée 9, 1700 Fribourg, Switzerland

[3]Centre for Research in Neuroscience, Department of Neurology and Neurosurgery, Research Institute of the McGill University Health Centre, Montreal General Hospital, 1650 Cedar Avenue, Montreal, QC H3G 1A4, Canada

Summary

Background: Excitatory synapses in the CNS are highly dynamic structures that can show activity-dependent remodeling and stabilization in response to learning and memory. Synapses are enveloped with intricate processes of astrocytes known as perisynaptic astrocytic processes (PAPs). PAPs are motile structures displaying rapid actin-dependent movements and are characterized by Ca^{2+} elevations in response to neuronal activity. Despite a debated implication in synaptic plasticity, the role of both Ca^{2+} events in astrocytes and PAP morphological dynamics remain unclear.

Results: In the hippocampus, we found that PAPs show extensive structural plasticity that is regulated by synaptic activity through astrocytic metabotropic glutamate receptors and intracellular calcium signaling. Synaptic activation that induces long-term potentiation caused a transient PAP motility increase leading to an enhanced astrocytic coverage of the synapse. Selective activation of calcium signals in individual PAPs using exogenous metabotropic receptor expression and two-photon uncaging reproduced these effects and enhanced spine stability. In vivo imaging in the somatosensory cortex of adult mice revealed that increased neuronal activity through whisker stimulation similarly elevates PAP movement. This in vivo PAP motility correlated with spine coverage and was predictive of spine stability.

Conclusions: This study identifies a novel bidirectional interaction between synapses and astrocytes, in which synaptic activity and synaptic potentiation regulate PAP structural plasticity, which in turn determines the fate of the synapse. This mechanism may represent an important contribution of astrocytes to learning and memory processes.

Introduction

Astrocytes are thought to play a crucial role in the development [1] and function [2] of synapses, which they envelop with their small peripheral tips [3]. Increasing evidence suggests the existence of bidirectional interactions between neurons and astrocytes at excitatory synapses, which has been coined the "tripartite synapse" [4]. Astrocytes display activity-mediated Ca^{2+} responses in vitro [5, 6] and in vivo [7, 8]. Ca^{2+} signals can trigger the release of gliotransmitters (glutamate, D-serine, ATP), which in turn regulate synaptic transmission [2]. Through these mechanisms, astrocytes have been proposed to play a critical role in modulating synaptic transmission [9, 10], plasticity properties [11–13], and long-term potentiation (LTP) [14], consistent with evidence suggesting that astrocytic Ca^{2+} transients can occur in spatially restricted areas [15, 16]. However, other studies have also proposed different mechanisms to account for a contribution of astrocytes to plasticity and memory [17, 18]. Additionally, recent studies also suggest that astrocytes could participate, during development, in the formation of synaptic networks by regulating synaptogenesis [19] and spine pruning [20]. Altogether, these data indicate an important functional role of astrocytes in their interactions with synapses, despite a lack of clear mechanistic insight.

Yet another intriguing property of perisynaptic astrocytic processes is their morphologically highly plastic nature [21]. Perisynaptic astrocytic processes (PAPs) express specific acting-binding proteins [22], and their plasticity may result in variable degrees of pre- and postsynaptic coverage of the synapse [23–25]. Therefore, the structural plasticity of PAPs may represent another aspect of the function of the tripartite synapse: synaptic activity may regulate astrocytic structural plasticity, which in turn may regulate the behavior and properties of synapses. To test this hypothesis, we performed time-lapse imaging of PAP structural dynamics in organotypic brain slices and in vivo. We further developed a new uncaging tool to selectively activate individual astrocytic processes and investigate the causal relationship between well-established synaptic plasticity paradigms, astrocytic motility, and synapse stability. We found that PAP structural plasticity is controlled by synaptic activity through Ca^{2+}-dependent mechanisms and that selective activation of PAP plasticity increased PAP coverage of spines and directly affected long-term spine survival. Finally, we show that this interaction between PAP structural dynamics and spine stability can also be functionally observed in the somatosensory cortex in vivo. We thus provide evidence for a novel bidirectional interaction between synapses and astrocytes in which synaptic activity and synaptic potentiation regulate PAP structural plasticity, which in turn determines the fate of the synapse. This attribute of the tripartite synapse may represent an important component of learning and memory, which highly relies on activity-dependent synapse rearrangements [26].

Results

Imaging of PAP Motility at Individual Synapses

To investigate the dynamics of PAPs around synapses, we expressed membrane-targeted farnesylated EGFP (EGFP-f) in CA1 neurons and farnesylated mCherry (mCherry-f) in stratum radiatum astrocytes of mouse hippocampal slice cultures using cell-specific strains of Semliki Forest virus [SFV(PD) and SFV(A7), respectively] [27, 28]. Putative contacts between dendritic spines and PAPs were imaged using confocal

*Correspondence: yann.bernardinelli@unige.ch

microscopy. Astrocytes could be identified by virtue of their complex morphology, which typically included extensive lamellipodia or sheet-like processes (Figure 1A; [29]). (Note that the color code is inverted in the figures.) All cells characterized as astrocytes were positively labeled for astrocytic markers glial fibrillary acidic protein (GFAP) and glutamine synthetase (see Figure S1 available online). Correlative confocal and 3D electron microscopy (EM) reconstructions confirmed the physical contacts between fluorescent PAPs and spines, indicating that confocal imaging reliably identifies PAPs that are in close apposition to synapses (Figure 1B; see also Movies S1 and S2).

Time-lapse confocal imaging of spine-PAP contacts revealed the motile nature of PAPs. It was characterized by continuous movements around spines over the time course of minutes (Figure 1C). These movements were quantified using a motility index (MI; Figure S2), similar to previously published methods [21, 30]. The PAP MI varied between spines (Figures 1D and 1E) but was inversely correlated with the initial PAP coverage of the spine (Figure 1D). Spines showing greater coverage had more stable PAPs (Figure 1D). In addition, PAP motility varied among spines that belonged to the same dendrite (Figure 1E), suggesting that the motility is synapse specific rather than dependent on global dendritic or astrocytic mechanisms.

Synaptic Activity Regulates PAP Motility through mGluRs and Intracellular Ca^{2+}

To assess the effect of synaptic activity on PAP movements, we first monitored PAP motility in the presence of either the cholinergic agonist carbachol, which induces theta activity [31], or the sodium channel blocker tetrodotoxin (TTX), which represses neuronal activity. The addition of carbachol significantly increased the MI, whereas TTX lowered the MI (Figure 2A), suggesting that neuronal activity was necessary and sufficient for PAP motility. To further test this possibility, we examined the effects of repetitive electrical stimulation of a group of Schaffer collaterals using a paired-pulse paradigm (10 min, 0.1 Hz, 50 ms interpulse interval). This stimulation protocol also increased the MI (Figure 2B), an effect readily observed at individual spines (Figure 2C). Increased motility was mediated by metabotropic glutamate receptors (mGluRs) since the addition of group 1 mGluR1,5 antagonists significantly reduced evoked PAP motility, similar to the addition of TTX (Figure 2B).

Since neuronal activity and Gq-coupled mGluR activation induce Ca^{2+} transients in PAPs [6, 15], we then tested the role of Ca^{2+} in PAP motility. To this aim, we examined the effects of calcium chelation on PAP motility by using 1,2-bis(2-aminophenoxy)ethane-*N*,*N*,*N*′,*N*′-tetraacetic acid acetoxymethyl ester (BAPTA-AM). We first verified that BAPTA-AM applied through bulk loading specifically localizes in astrocytes as suggested by others [32]. Ca^{2+} events of BAPTA-AM-loaded slices were monitored in astrocytes using Fluo-4 and in pyramidal neurons using Lck-GCamp3 [33] (Figure S3; Movie S3). The chelation of intracellular calcium (Ca^{2+}_i) by BAPTA-AM prevented ATP-mediated calcium transients in astrocytes (Figure S3A), but it did not affect carbachol-induced calcium spiking in neurons (Figure S3B). Also, BAPTA-loaded astrocytes showed a significantly lower PAP motility than control astrocytes (Figure 2A), suggesting that PAP motility is regulated through Ca^{2+}. We then selectively induced Ca^{2+} transients in astrocytes using the astrocyte-specific expression of exogenous Gq-coupled receptors of the *Mas-related gene* family (MrgA1 and MrgC11 [34, 35]; Figure 2D) combined with the bath application of the MrgA1 agonist peptide Phe-Met-Arg-Phe-NH_2 (FMRFa) [34]. This induced both Ca^{2+}_i transients (Figures 2E and 2F) and an increase in PAP motility in the infected astrocytes (Figure 3G). Altogether, these experiments indicate that PAP motility depends on Ca^{2+} events that are induced by synaptic activity, possibly through Gq-coupled receptors such as mGluRs.

Synaptic Potentiation Results in a Biphasic Change in PAP Motility and an Increase in PAP-Spine Coverage

The increase in PAP motility in response to synaptic stimulation raises the possibility that synaptic potentiation, i.e., a phenomenon induced by patterns of high-frequency activity, could induce changes in PAP motility and morphology. To test this, we applied a short theta-burst stimulation (Θ_{burst}) protocol (five trains at 5 Hz of four 100 Hz pulses, repeated twice with a 10 s interval) that has been shown to induce LTP in hippocampal slice cultures [31] (Figure 3A). Similarly to low-frequency stimulation, Θ_{burst} stimulation significantly increased PAP motility (Figure 3A). Comparably to what was observed with low-frequency stimulation, the group 1 mGluR1,5 antagonists also blocked the motility increase in this paradigm. Postsynaptic activation was not required for the effect, as the glutamate receptor antagonists D-AP5 and NBQX did not prevent the Θ_{burst}-induced increase in MI (Figure 3A), suggesting that glutamate release directly modulated PAP motility.

Synaptic LTP is known to lead to an increase in size of activated spines [31, 36]. This provided us with a tool to check whether synaptic potentiation-induced increased PAP motility is synapse specific. We first confirmed that the application of LTP-inducing Θ_{burst} stimulation induced spine head enlargements (of more than 20% growth in size). Indeed, 30 min poststimulus, we found 40% of the spines to be enlarged [31] (Figure 3B). This effect was blocked by the NMDAR blocker D-AP5 (Figure 3B), indicating that Θ_{burst} stimulation produced genuine postsynaptic, NMDAR-dependent LTP. Interestingly, spine enlargement was prevented by mGluR antagonists (Figure 3B). Θ_{burst} stimulation also increased the number of spines exhibiting an increased coverage by PAPs (Figure 3C). The increased coverage preferentially occurred on spines that had enlarged (Figure 3D) and was blocked by mGluR antagonists (Figures 3C and 3D).

We next investigated the temporal changes in PAP motility that follow LTP induction. Whereas PAP motility was found to be increased 10 min after Θ_{burst} stimulation (Figures 3A and 3E), PAPs had become greatly stable after 30 min poststimulus. Remarkably, this effect preferentially occurred around enlarged spines (Figure 3E). The motility of PAPs around nonenlarged spines remained unchanged, suggesting that the increased spine coverage was the result of the selective changes in PAP motility around spines that were potentiated. This LTP-associated reduction of PAP motility was also prevented by mGluR blockade (Figure 3E). These results indicate that Θ_{burst} stimulation transiently enhances PAP motility, which presumably leads to a PAP repositioning, subsequent stabilization, and increase in the PAP coverage of potentiated synapses.

Activation of PAPs at Single Synapses Increases Spine Coverage and Stability

To further test whether locally evoked Ca^{2+} transients in PAPs could regulate motility in spatially defined domains, we developed a photoactivation tool based on Mrg receptors to

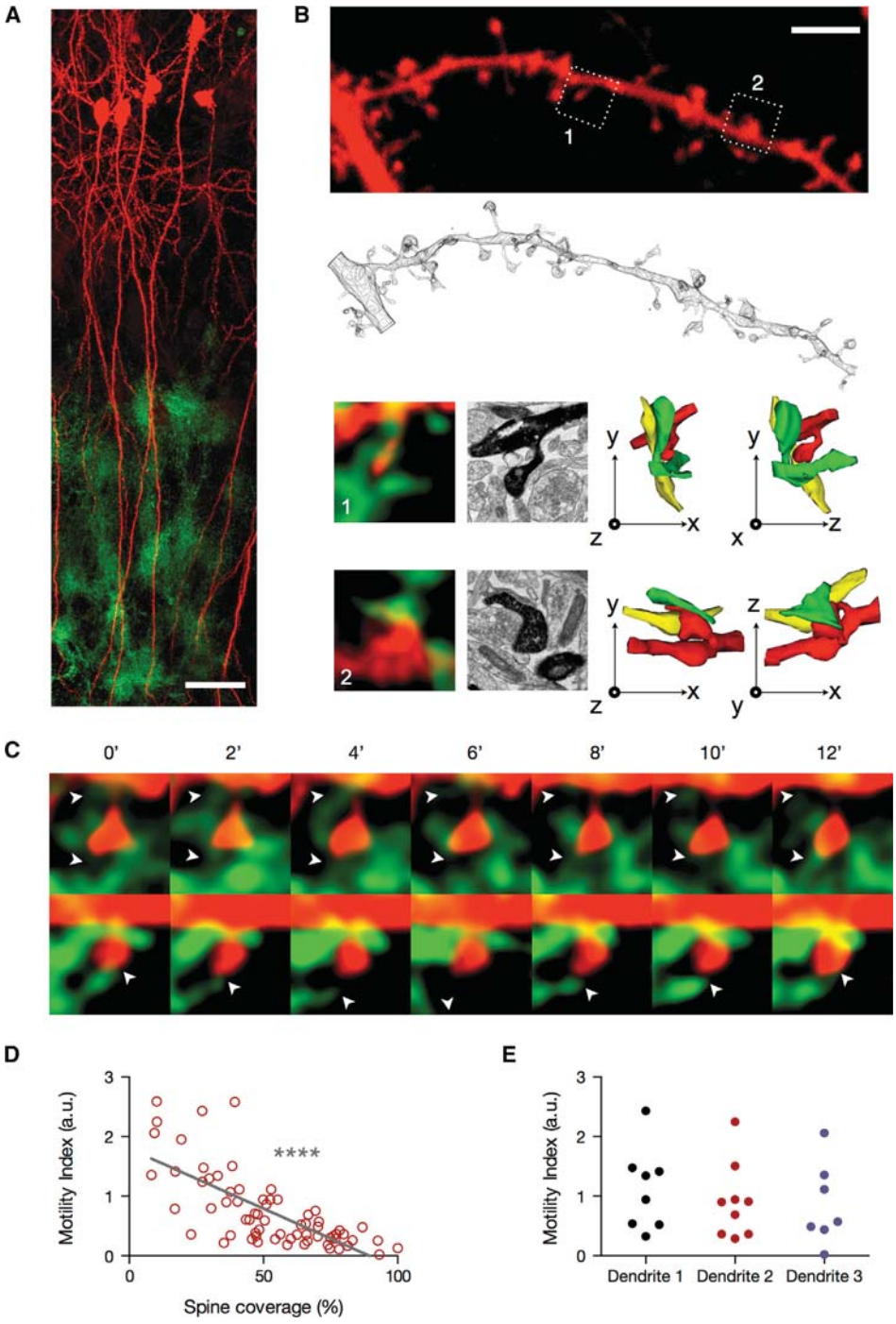

Figure 1. Imaging of PAP Motility around Synapses

(A) z stack projection of confocal images showing CA1 pyramidal neurons infected with SFV(PD)-EGFP-f (red) and stratum radiatum glial cells infected with SFV(A7)-mCherry-f (green; see Figure S1). Scale bar, 100 μm.

(B) Top: illustration of a labeled dendritic segment with spines contacted by labeled astrocytes (not shown for clarity; scale bar, 5 μm). This dendritic segment was then 3D reconstructed from serial EM (drawing below). The spines in the dotted square boxes on the dendritic segment are shown below this reconstruction with their neighboring PAPs (green, 1 and 2). Black and white pictures are EM images of the same synapses (intense black: DAB-labeled dendritic segment). On the far right are 3D reconstructions from serial EM showing the same postsynaptic spines (red), terminals (yellow), and PAPs (green) in different orthogonal projections. Scale, 3 μm square boxes. See Movies S1 and S2.

(C) Time-lapse of spine-PAP pairs recorded every 2 min showing basal PAP movements (white arrowheads highlight noteworthy PAP movements).

(D) Motility index (MI) calculated for individual spines (see Figure S2). Spine coverage was plotted against MI, showing a highly significant inverted correlation. Gray line: linear regression ($y = -0.02 * x + 1,797$). Correlation statistics: Pearson correlation test, $n = 70$.

(E) MI calculated for every spine-PAP contact found in three different dendritic sections. MI is highly heterogeneous from spine to spine ($n1 = 8$, $n2 = 9$, $n3 = 7$).

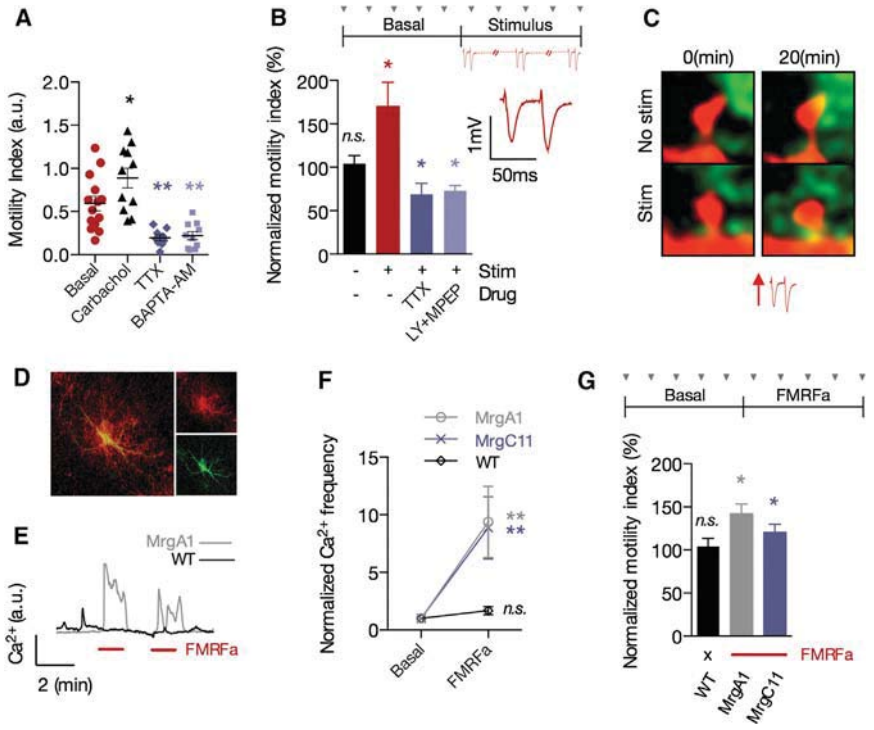

Figure 2. Neuronal Activity and Astrocytic Ca^{2+} Modulate PAP Motility

(A) PAP MI under basal conditions (circles, n = 14), after application of carbachol (50 μM, n = 11; see Movie S3) or TTX (1 μM, n = 9), or after BAPTA-AM (100 μM, n = 10; see Figure S3) bulk loading (one-way ANOVA with Dunnett's posttest).

(B) Spine-PAP pairs were imaged repetitively every 2 min (arrowheads in time line) for 10 min before (basal) and 10 min during continuous stimulation of Schaffer collaterals (stimulus, 0.1 Hz, paired stimuli at 50 ms interval). The graph shows the changes in MI measured during stimulation and normalized in each experiment to the values obtained during the basal period. The normalized MI was measured without stimulation (black, n = 7), with stimulation (red, n = 7), with stimulation and TTX (dark blue, n = 7), or with stimulation and LY367385 ([LY] 100 μM) + 2-methyl-6-(phenylethynyl)-pyridine ([MPEP] 50 μM, light blue, n = 7, paired t test). Inset shows evoked EPSPs.

(C) Spine-PAP pairs imaged before and after stimulation protocol without (top) and with (bottom) stimulation showing that PAP movements were increased upon neuronal stimulation.

(D) Astrocytes infected with SFV(A7) driving the genes of MrgA1 tagged with MycHis, an internal ribosome entry site sequence and mCherry-f. Images show mCherry-f (top right, red), immunofluorescence against MycHis (bottom right, green), and an overlay (left).

(E) Representative traces of astrocytic Ca^{2+} changes monitored with Fluo-4 following two consecutive bath applications of FMRFa (red bars) in MrgA1-infected (gray trace) and in wild-type (WT) astrocytes (black trace).

(F) Frequency of Ca^{2+} events calculated before (basal) and during FMRFa application (FMRFa) in MrgA1-expressing astrocytes (gray circle, n = 4) or MrgC11-expressing astrocytes (blue cross, n = 4) as well as noninfected astrocytes (black diamond, n = 4, paired t test).

(G) Increased PAP MI normalized to basal conditions (basal, time line, top scheme) induced by FMRFa (15 μM) in MrgA1-expressing astrocytes (gray bar, n = 9) and MrgC11-expressing astrocytes (blue bar, n = 6), but not in noninfected astrocytes (black bar, n = 7) (t tests).

Data are represented as means ± SEM.

locally trigger calcium events in PAPs. We focused on the Mrg member of Gq-coupled receptors MrgC11. As observed above for MrgA1, when transfected in astrocytes, activation of MrgC11 by application of the FMRFa agonist triggered calcium transients. Interestingly, MrgC11 has known silent mutants (MrgC11Y110A [MrgC11-Tyr] [37] and MrgC11D179A [MrgC11-Asp] [37]) that could be used as negative controls. Indeed, astrocytes infected with the silent mutants of MrgC11 were unable to generate Ca^{2+} spikes in response to FMRFa (Figure 4A). This indicates that the MrgC11 receptors system constitutes a powerful tool to generate Ca^{2+} spikes in astrocytes.

In order to be able to activate PAPs at single synapses in a spatially and temporally restricted manner, we developed a caged-FMRFa (FMRFa-NVTEG; Figure 4B) for single- and two-photon (2P) flash photolysis. Bath application of FMRFa-NVTEG to MrgA1-infected astrocytes did not elevate Ca^{2+}, confirming that the caged peptide was inactive in its non-cleaved form (Figure 4C). In contrast, 365 nm UV flashes [38] induced robust Ca^{2+} spikes (Figure 4D).

We then tested the effects of Mrg receptor activation on PAP motility at the single-synapse level. 2P uncaging of FMRFa-NVTEG on PAPs near spines significantly increased the motility of MrgC11-expressing astrocytes but not of $MrgC11^{mut}$ astrocytes (Figure 5A). Additionally and consistent with the Θ_{burst} experiments, photoactivated spine-PAP pairs displayed an increased spine coverage 10–30 min after photolysis (Figure 5B). This was not observed with nonflashed, neighboring spine-PAP pairs on the same dendrite (Figure 5B).

To further investigate the relations between PAP structural changes, synaptic function, and stability, we tracked the interaction between PAPs and spines over the first 24 hr after 2P uncaging. We compared on the same dendritic segment spine-PAP pairs that were photoactivated with others that were not. Spines in contact with photoactivated PAPs were more likely to be present 24 hr later than those surrounded with nonactivated PAPs (Figures 6C and 6D). This effect was not observed in PAPs expressing $MrgC11\text{-}Asp^{mut}$. Thus, spatially restricted activation of metabotropic receptors was sufficient to increase PAP motility, promote the repositioning of PAPs around the spine, and increase the stability of the synapse.

In Vivo PAP Motility Is Influenced by Neuronal Activity, Correlates with Spine Coverage, and Predicts Spine Stability

Next, we wondered whether PAP motility could also be observed in vivo and serve similar functions. We used adenoassociated virus (AAV) to selectively drive expression of mCherry-f in PAPs of adult transgenic mice expressing GFP in sparse subsets of cortical neurons. We performed 2P laser scanning microscopy through a cranial window preparation [39] to monitor, within layer 1, the motility of mCherry-labeled PAPs juxtaposed to spines present on the apical dendritic tufts of EGFP-expressing L5b pyramidal neurons. Repetitive imaging of PAPs around individual spines showed a level of motility very similar to what was observed in vitro, with a spine to spine variability (Figures 6A and 6B). In addition,

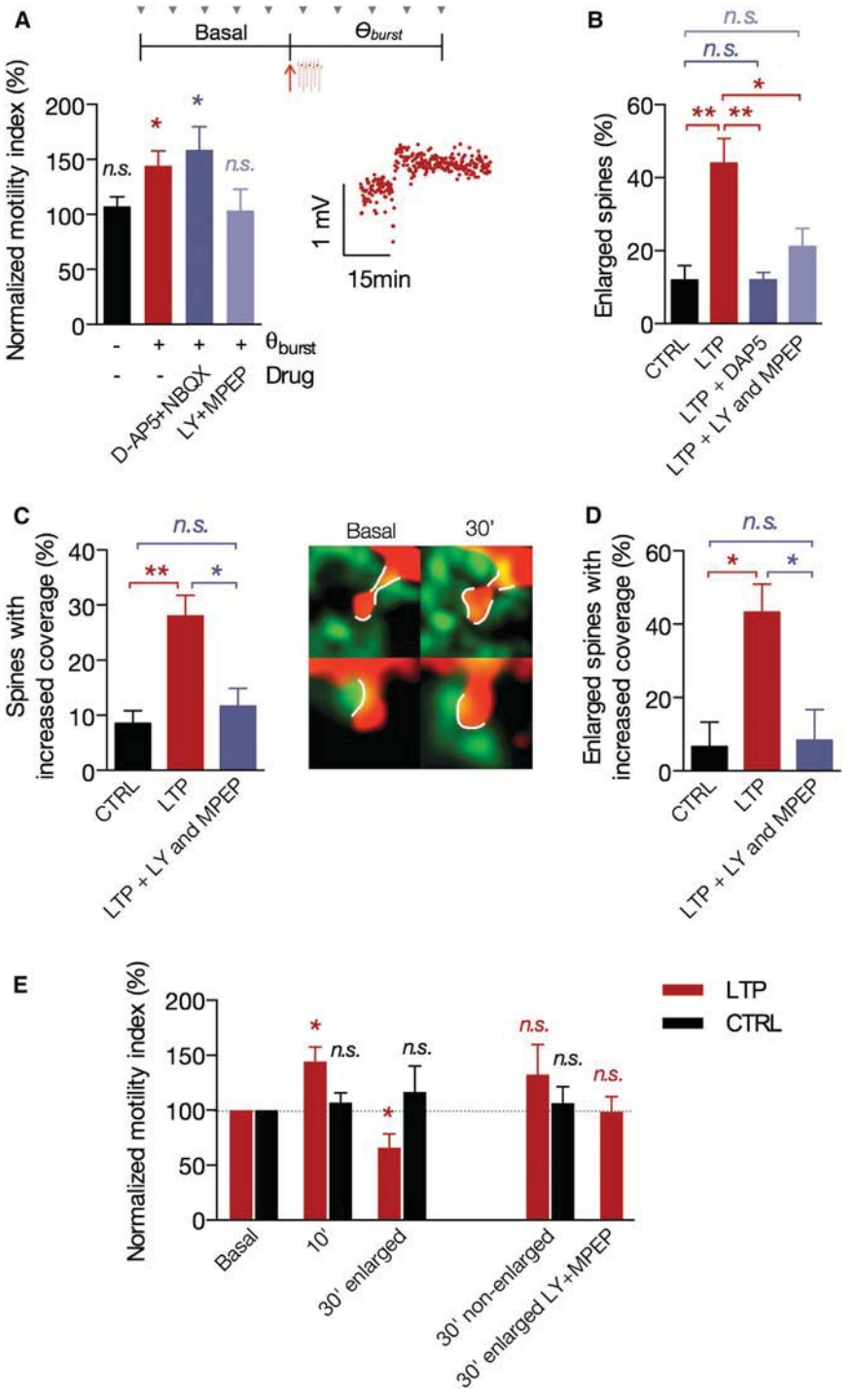

Figure 3. Synaptic Potentiation Induces a Biphasic Change in PAP Motility and Elevates Spine Coverage

(A) Spine-PAP pairs were imaged 10 min before (basal) and 10 min after a Θ_{burst} protocol (top, time line). The MI was measured without Θ_{burst} stimulation (black, n = 7), during the 10 min that followed Θ_{burst} stimulation (red, n = 7), and with Θ_{burst} stimulation and either NBQX (1 μM) and D-AP5 (50 μM, dark blue, n = 7) or LY367385 and MPEP (light blue, n = 7, paired t test). Inset: increase in evoked EPSPs slope produced by Θ_{burst} stimulation.

(B) Proportion of spines that enlarge over a period of 30 min without Θ_{burst} stimulation (control [CTRL], black, n = 5), after Θ_{burst} stimulation (LTP, red, n = 5), after Θ_{burst} stimulation + D-AP5 (dark blue, n = 5), and after Θ_{burst} stimulation + LY (100 μM) + MPEP (50 μM) (light blue, n = 6, one-way ANOVA with Bonferroni posttest).

(C) Percentage of spines increasing their coverage by PAP following LTP induction by Θ_{burst} stimulation (n = 5), under CTRL conditions (n = 5), and with LY + MPEP (blue, n = 6, one-way ANOVA with Bonferroni posttest). Boxes: two spine-PAP pairs are illustrated before (left) and 30 min after (right) Θ_{burst} stimulation. Note the spine enlargement and the increased PAP coverage (white line).

(D) Proportion of enlarged spines that also displayed an increased coverage under control conditions (CTRL, n = 5), following LTP induction (n = 5), and with LY + MPEP (blue, n = 6, one-way ANOVA with Bonferroni posttest).

(E) PAP MI around enlarged spines before, 10 min, and 30 min after Θ_{burst} stimulation (LTP, red, n = 6) and without stimulation (CTRL, black, n = 5). No changes in MI were detected at nonenlarging spines in both CTRL and LTP conditions, or at enlarging spines when Θ_{burst} stimulation was applied with mGluR1,5 blockade (LY + MPEP, n = 6, paired t test).

Data are represented as means ± SEM.

similar to what was seen in brain slices, spine motility was inversely correlated with the level of spine coverage by PAPs (Figure 6B). We next investigated whether neuronal activity could drive PAP motility in vivo. PAP movements around spines were monitored for two consecutive 10 min periods, as performed in vitro. Here, the first 10 min basal period was followed and compared to a 10 min period during which neuronal activity was increased through whisker stimulation protocol. Remarkably, stimulation of the whisker corresponding to the whisker barrel in which MI was monitored (principal whisker) resulted in an increased MI, whereas the stimulation of the surrounding whisker failed to increase the MI (Figure 6C). This indicates that neuronal activity specifically drives the motility of astrocytic processes around synapses within the stimulated barrel column in anesthetized adult mice. Finally, PAP motility was significantly lower at spines that persisted over 4 days than at spines that would disappear before the next imaging session (Figure 6D). Taken together, these data suggest that spine stability in vivo is also closely correlated to PAP motility and PAP spine coverage.

Discussion

Here we describe a novel bidirectional role of PAPs in the tripartite synapse. PAPs are highly motile structures, to an even higher degree than dendritic spines [21]. Our data suggest that PAP motility is regulated by synaptically released glutamate through activation of PAP mGluRs and the generation of Ca^{2+} transients. This is likely to occur at individual

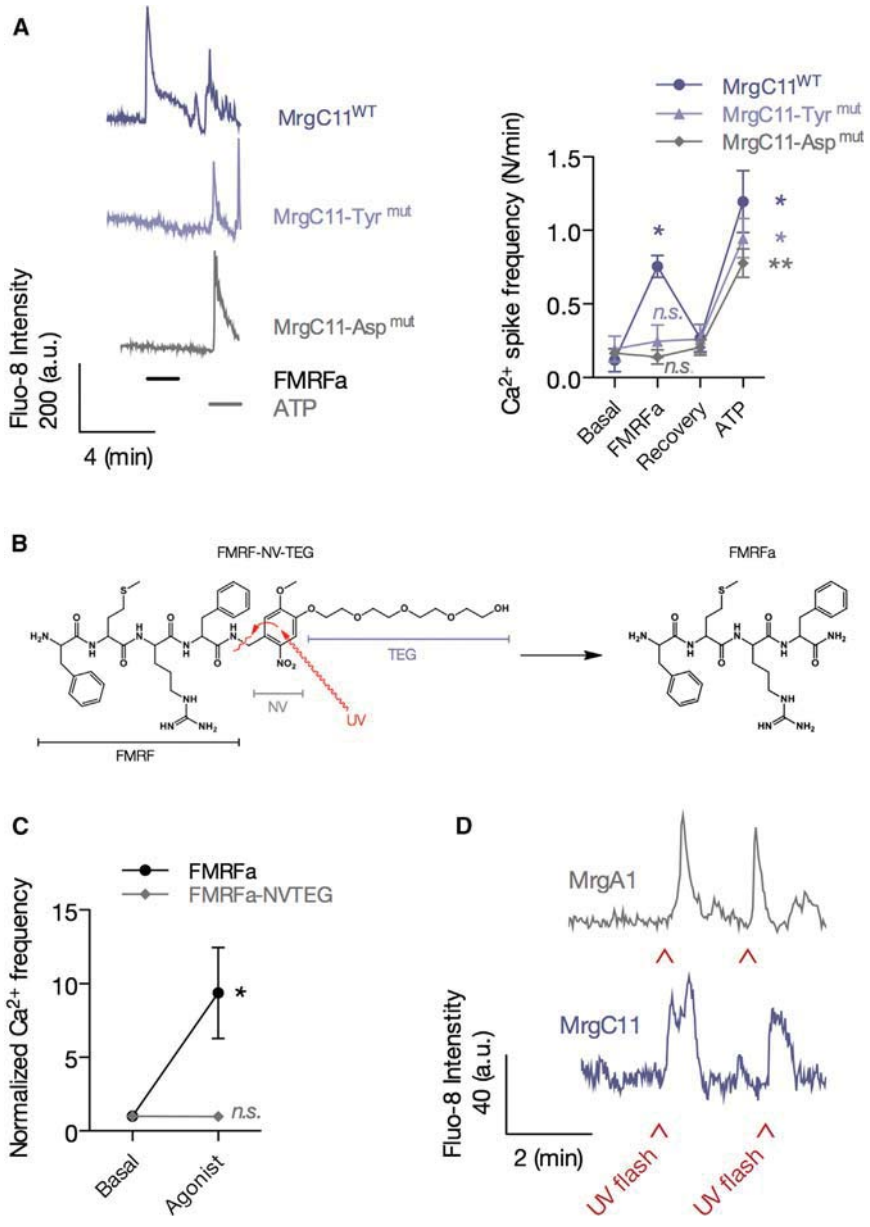

Figure 4. Development of a Flash Photolysis System for the Spatial and Temporal Induction of Astrocytic Calcium Transients

(A) Ca^{2+} traces (left) and quantification of Ca^{2+} spike frequency (right) during FMRFa (15 μM) or ATP (100 μM) application in PAPs transfected with $MrgC11^{WT}$ (n = 4) and $MrgC11^{mut}$ ($MrgC11\text{-}Tyr^{mut}$ and $MrgC11\text{-}Asp^{mut}$; n = 4, paired t test; regions of interest were picked in the whole astrocyte body, including processes).

(B) Photolysis reaction of FMRFa-NVTEG.

(C) FMRFa-NVTEG, when bath applied, did not increase the frequency of Ca^{2+} spikes in MrgA1-astrocytes (gray diamonds, n = 3), while FMRFa did (circles, n = 4, paired t test).

(D) The traces show Ca^{2+} transients evoked by single-photon uncaging (365 nm) of FMRFa-NVTEG (red arrowheads) on MrgC11-infected and MrgA1-infected astrocytes.

Data are represented as means ± SEM.

synapses, as LTP-induced PAP motility selectively modified the structural organization and spine coverage around potentiated synapses, which in turn was associated with an increased stability of synapses. Thus, in addition to regulating glutamate transport [40], the release of gliotransmitters [41], and neurometabolic coupling [42], astrocytic Ca^{2+} dynamics are important to regulate PAP motility and thereby the stability of the tripartite synapse. These results provide a new mechanism through which synaptic activation can control the physical interactions between PAPs and excitatory synapses, and they demonstrate an important structural role of PAPs as active partners in the regulation of activity-dependent synaptic remodeling.

Learning and memory processes in cortex and hippocampus occur through both functional and structural mechanisms. It is largely accepted that a first step is a functional potentiation of synaptic transmission, mainly due to the recruitment of α-amino-3-hydroxy-5-methylisoazol-4-propionate receptor (AMPAR) at postsynaptic spines [43]. Structural mechanisms are less understood, and their causal link to functional mechanisms is still unclear. Current concepts of synapse structural plasticity propose that following LTP induction paradigms, postsynaptic spines increase their turnover and that the subset of spines that have been functionally potentiated become very stable structures that persist over days [31, 44, 45]. The mechanisms promoting spine stability remain largely unknown and could involve astrocytic perisynaptic processes, as they are known to increase their synaptic coverage after LTP [24] and are functionally implicated in LTP mechanisms [14, 18]. Here, we show that PAP motility could be triggered by brief LTP-inducing protocols, which had a biphasic effect: the initial increase in motility was followed by a stabilization of PAP movements associated with an enhanced physical coverage of the synapse. This in turn was associated with an increase in spine stability. Astrocytes remodeling might thus be required for activity-dependent synapse stabilization, in addition to other synapse-specific, D-AP5-sensitive mechanisms. This result is consistent with previous EM studies showing changes in astrocytic coverage following activity [24, 25]. This strongly suggests that the role of this LTP-induced increase in motility was to allow a repositioning of PAPs around activated synapses. This is supported by the observation that blockade of PAP motility by mGluR antagonists prevented repositioning, while conversely, a transient increase in PAP motility by exogenous metabotropic receptor activation resulted in an increased coverage of the synapse. Note that group 1 mGluR antagonists also interfere with LTP [46] and prevent activity-mediated spine enlargement and stabilization [47]. Enhanced PAP motility is thus required for restructuring PAP-spine contacts. In the long term, however, LTP resulted in a reduced motility, and spines with a low PAP motility were also those that showed an increased coverage by PAPs and

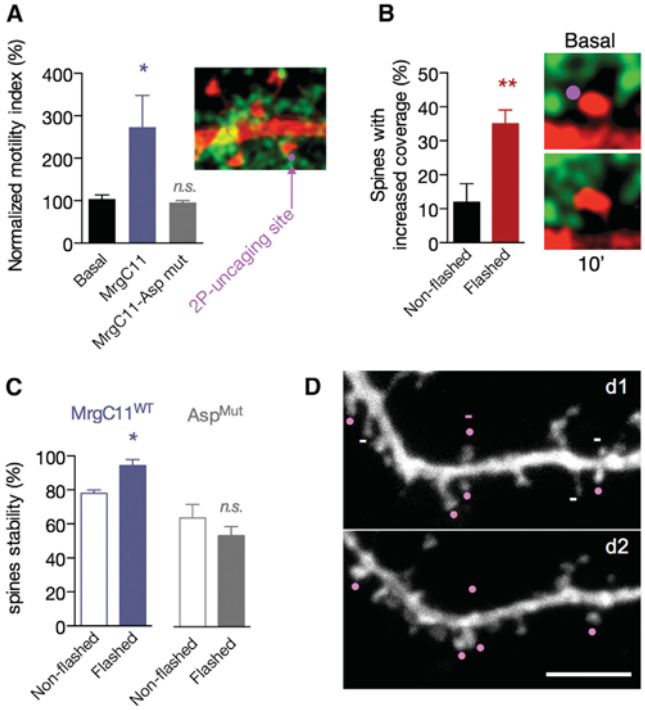

Figure 5. Local PAP Activation Enhances Spine Coverage and Long-Term Spine Stability

(A) 2P uncaging (725 nm) of FMRFa-NVTEG at spine-PAP pairs increased MI in MrgC11^{WT} (blue, n = 7) but not in MrgC11-Asp^{mut} (gray, n = 8, paired t test)-infected astrocytes. The image illustrates an MrgC11-infected astrocyte (green) and a PAP activated by 2P uncaging (pink dot).

(B) 2P uncaging of FMRFa-NVTEG increases MrgC11-PAP coverage of spines 10 min after photolysis (red, n = 5) compared to nonflashed spines (black, n = 5, nonparametric t test). The pictures show an illustration of spine coverage before and 10 min after photolysis.

(C) Increase in 24 hr spine stability at flashed MrgC11^{WT}-PAP-spine pairs (blue, n = 7 [35 spines]) versus nonflashed pairs (open blue, n = 7 [162 nonflashed spines]). In contrast, flashed MrgC11-Asp^{mut}-PAP-spine pairs (gray, n = 5 [19 spines]) showed no changes compared to nonflashed pairs (open gray, n = 5 [113 spines], nonparametric t test).

(D) Dendritic segment illustrating 2P-flashed spine-PAP pairs (pink dots, d1) and their survival 24 hr later (d2) (note the disappearance of spines, indicated by −). Scale bar, 10 μm.

Data are represented as means ± SEM.

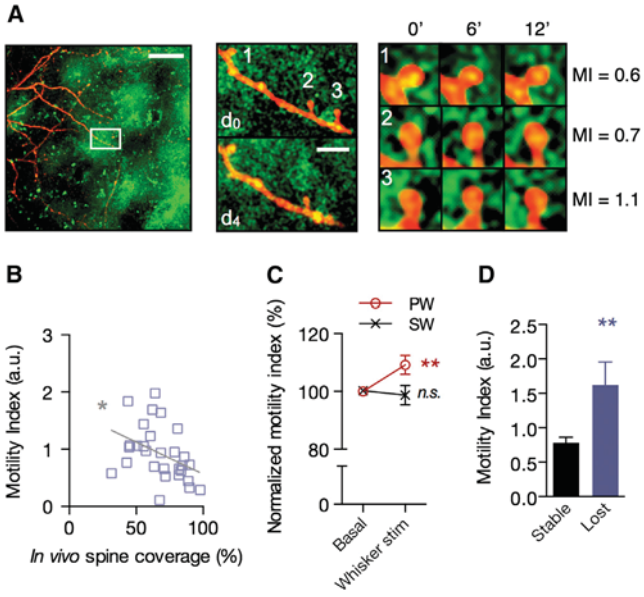

Figure 6. The Motility of Cortical Astrocytic Processes Predicts Spine Fate In Vivo

(A) Left: z stack projection of 2P confocal images showing a layer 5 pyramidal neuron distal dendritic branch (red) in layer 1 of the mouse somatosensory cortex in vivo. Astrocytes were infected with AAV2/5-GFAP-mCherry-f (green). Scale bar, 50 μm. Layer 5 cells express GFP. The images are colored inversely to match the in vitro figures. Middle: higher magnification of a dendritic segment and its surrounding infected astrocyte (white box) imaged at day 1 (d_0) and 4 days later (d_4). Scale bar, 5 μm. Right: MI of three PAPs around labeled spines illustrated and quantified at d_0. Scale, 3 μm square boxes. Spine 3 with the higher MI disappeared on d_4.

(B) PAP MI in layer 1 barrel cortex in vivo (blue squares, n = 28, four mice) is correlated with spine coverage (n = 29, Pearson correlation test).

(C) PAPs were imaged 10 min before (basal) and 10 min after (whisker stim) principal whisker (red circle, n = 15, three mice) or surrounding whisker (black cross, n = 13, three mice) stimulation (8 Hz).

(D) PAP MI of stable (black, n = 19 spines, four mice) and lost spines (blue, n = 12 spines, four mice).

Data are represented as means ± SEM.

a better stability under in vitro and in vivo conditions. Thus, a low PAP motility favors spine persistence. Interestingly, it was recently found that increased synaptic activity could promote engulfment and elimination of excitatory synapses by astrocytic processes [20]. Although PAP motility was not specifically assessed in these experiments, this suggests that astrocytic processes, depending on their level of activation and interaction with synapses, could contribute either to spine pruning and elimination or to long-term spine persistence. Thus, in addition to their role in synaptogenesis [48, 49], astrocytes could also have a critical function in the process of synapse selection taking place during the development of synaptic networks [50, 51] and the rewiring observed during LTP [26].

Exactly how the structural reorganization of PAPs around synapses could contribute to their stability remains unclear at present. Previous work has suggested that adhesion molecules, by increasing transsynaptic cohesion via N-cadherin [52] or PAP-synapse sticking through EphA4/ephrin-A3 contacts [17, 53], could play a role in activity-dependent synapse stability. Here, we propose that PAPs could promote structural interactions and molecular communication between synaptic partners through their reduced motility and increased coverage of the synapse. This may affect functional parameters such as the number and/or distribution of glutamate transporters [25], but also physical links between PAPs and synaptic partners. Synaptic coverage and PAP movements are correlated with spine stability, as shown in the present paper. Thenceforth, molecular mechanisms driving PAP motility would indirectly impact spine stability. This could be the case with the acting-binding proteins Profilin-1 [54] or Ezrin [22] together with calcium excitability of astrocytic processes, which may serve to modify PAP structure in an activity-dependent manner.

A very important aspect of the present finding is that PAP structural plasticity and its consequences on synapse stability operate at the level of individual synapses. Astrocytes can contact up to 100,000 synapses [55], and while they may work as a syncytium propagating calcium waves over long distances [7, 56], it has been proposed that they might be able to differentiate between individual inputs [57]. Our experiments using single-synapse photoactivation show that the regulation of PAP motility and synapse stability is synapse

specific, consistent with the notion that Ca^{2+} transients can occur in defined microdomains of astrocytic processes [15, 16, 29, 58]. Through these spatially restricted mechanisms, astrocytes can participate in controlling the function and stability of individual synapses and thereby contribute to the specificity of learning-related structural rearrangements [26]. This could represent a key mechanism to account for the newly identified functional role of astrocytes in learning and memory processes [14, 18].

Experimental Procedures

Organotypic Hippocampal Slice Preparation

Organotypic hippocampal slices cultures were prepared as described previously [31]. In vitro protocols were approved by the Geneva Veterinarian Office (authorization 31.1.1007/3520/0 to D.M.). Briefly, 400 μm-thick hippocampal slices were prepared from postnatal day 6–7 C57BL/6J mice and transferred onto 0.4 μm-pore-size culture membranes (Millipore). Slices were cultured for 7–21 days in vitro. Culture medium consisted of 50% minimum essential medium, 25% horse serum, 25% Hank's balanced salt solution, 6.5 mg/ml D-glucose, and 0.5% penicillin/streptomycin.

SFVs, AAV, and Plasmids

For expressing fluorescent proteins, Mrg receptors, or Ca^{2+}-sensitive proteins in hippocampal slices, SFVs were created as described previously [21]. DNAs were cloned into SFV(A7) for expression in astrocytes or into SFV(PD) for expression in neurons. In vivo infection of astrocytes was performed using AAV2/5-GFAP-mCherry-f-WPRE virus (see Supplemental Experimental Procedures for DNA cloning and virus creation).

Immunohistochemistry

See Supplemental Experimental Procedures.

Electron Microscopy

For the correlative confocal and EM analysis, slice cultures with fluorescent neurons and surrounding fluorescent PAPs were first imaged with confocal microscopy. Immediately after imaging, slices were fixed, cryoprotected, and stained with antibodies prior to 3,3′-diaminobenzidine (DAB) staining and EM imaging. See Supplemental Experimental Procedures for details.

Electrophysiology

Slice cultures were maintained at 32°C in an interface chamber under artificial cerebrospinal fluid (ACSF) perfusion. Excitatory postsynaptic potentials (EPSPs) were evoked by stimulation of a group of Schaffer collaterals and recorded in the CA1 region with 2–5 MΩ pipettes filled with ACSF. Potentiation was analyzed by measuring EPSP slopes expressed as percent of baseline values using an acquisition program written with Igor Pro (WaveMetrics). LTP was induced by Θ_{burst} stimulation (five trains at 5 Hz composed each of four pulses at 100 Hz, repeated twice at 10 s intervals). Paired pulses (two pulses, 50 ms interval, 0.1 Hz) and Θ_{burst} stimulation during imaging were performed in immersion and superfusion conditions.

Calcium Imaging

Ca^{2+} measurements in astrocytes were performed by bulk loading of the Ca^{2+}-sensitive dyes Fluo-4 (Invitrogen) or Fluo-8 (Teflabs). Ca^{2+} measurements in neurons were performed with SFV(PD) Lck-GCaMP3. See Supplemental Experimental Procedures for further explanations.

Spine-PAP Imaging in Organotypic Hippocampus

Viral gene delivery of farnesylated fluorescent proteins EGFP-f and mCherry-f was used to separately label astrocytic and neuronal membranes. SFVs were injected into mice hippocampal organotypic cultures. SFV(PD) was injected in the CA1 pyramidal layer and SFV(A7) in the CA1 stratum radiatum. Time-lapse imaging was performed 12–24 hr after virus injection (see Supplemental Experimental Procedures for imaging conditions). Primary, secondary, or tertiary dendritic segments located in the stratum radiatum containing about ten spine-PAP contacts were chosen for both MI and morphological analyses. z stacks of spine-PAP pairs were acquired every 2 min during two consecutive 10 min periods (see Figure 2B). For quantification of PAP motility, a motility index modified from [21] was computed offline (see Supplemental Experimental Procedures for MI calculation details).

24 hr spine stability was analyzed for all protrusions independently of their shape. Stable spines between 0 and 24 hr time points were counted, subdivided into two populations (flashed and nonflashed), and divided by the total number of spines in their categories. In each experiment, five spines were photoactivated. Spine coverage analysis was performed by measuring the fraction of spine perimeter showing spine-PAP apposition. Spine-PAP apposition was calculated by measuring manually the length of spine-PAP contacts from the spine neck to the spine head on individual z planes displaying the highest proportion of contacting membranes. Spine perimeter was calculated in the same z plane. Both perimeters were measured before and after the experimental paradigm. All spine-PAP contacts on a dendritic segment were considered for analysis. All morphological analyses were carried out in a blind manner.

Synthesis of Caged FMRFa

Nitroveratryl photolabile protecting group (NV) was chosen as the cage. Its high quantum yield and absorption maximum make it very suitable for experiments with very short irradiation times such as 2P flash photolysis. Moreover, NV can be coupled to a carboxylic acid, thus allowing the amide group to be released after photolysis. These NV properties permitted synthesis of the caged compound using as a start point the easily accessible FMRF tetrapeptide (Equation 1, Synthetic and Photolytic Pathways).

$$\mathrm{FMRFOH} + \mathrm{NVNH_2} \xrightarrow[\text{agents}]{\text{coupling}} \mathrm{FMRFa\text{-}NV} \xrightarrow{h\nu} \mathrm{FMRFa}$$

To increase the solubility of the end product, we synthesized another analog, bearing a tetraethyleneglycol (TEG) function. The obtained caged peptide (FMRFa-NVTEG) showed good solubility in water and physiological medium. The 360 nm irradiation wavelength showed the rapid liberation of FMRFa molecules, with a quantum yield value of 0.023, which is consistent with similar compounds [59] and elevated for an organic compound.

Flash Photolysis

Single-photon flash photolysis was modified from [60]. A high-power 365 nm LED (NCSU033B, Nichia) mounted into an LED driver (Migthex) was delivered to the sample through an optical fiber equipped with a condenser (Siskiyou) (see Supplemental Experimental Procedures). FMRFa-NVTEG uncaging was performed on the stage of an Olympus FluoView 300 system with a 2P laser (Cameleon, Coherent) and 40× 0.8 numerical aperture immersion objective following the previously published protocol for MNI-glutamate uncaging [61] (see Supplemental Experimental Procedures).

In Vivo Imaging

C57BL/6J transgenic mice expressing EGFP under control of the Thy-1 promoter (GFP-M line [39]) were used. Four adult animals (age 2–4 months) of either sex were used (see Supplemental Experimental Procedures for surgery, anesthesia, and virus injection information). In each animal, two dendrites running tangentially to the imaging plane in L1 (<100 μm deep) were selected from regions where PAP labeling was present. Tracking the dendritic structures down to their somas revealed that all selected dendrites originated from pyramidal neurons located within L5. Image stacks (50 × 50 μm, 1 μm steps between planes) of dendritic segments and neighboring astrocytes, with a resolution of 0.1 μm/pixel and 3.9 μs dwell times, were repeatedly acquired every 2 min for a total of 20 min per imaging session. Imaging sessions were spaced 4 days apart. Spines were scored as described previously [39]. In vivo protocols were approved by the Geneva Veterinarian Office (authorization 1007/3668/2 to A.H.).

In Vivo Whisker Stimulation

The whisker barrel column in which the L5b pyramidal neuron of interest was located (principal barrel) was identified using intrinsic optical signal (IOS) imaging. The whisker corresponding to this barrel was defined as the principal whisker. The surrounding whisker corresponded to a whisker barrel that was located at least two barrels away from the principal whisker barrel. All whisker stimulation experiments were performed under medetomidine/midazolam/fentanyl (0.21, 5, and 0.05 mg/kg, respectively) mixed anesthesia. Image stacks (50 × 50 μm, 1 μm steps between planes) of dendritic segments and neighboring astrocytes, with a resolution of 0.1 μm/pixel, 3.9 μs dwell times, were repeatedly acquired every 2 min for a total duration of 30 min. After a 10 min baseline, either the principal or surrounding whisker was continuously stimulated for 10 min with a piezoelectric device at a frequency of 8 Hz, during which stacks were acquired. In order to prevent artifacts due

to potentiation of the principal barrel, surrounding and principal whisker stimulation was performed on separate days, and the surrounding whisker was always stimulated prior to the principal whisker.

Statistics

For morphological measurements (coverage and stability), n represents the number of dendritic segments analyzed (containing at least ten spine-PAP pairs); only one dendritic segment was analyzed per hippocampal slice. For MI measurements, n corresponds to a single spine-PAP pair. A maximum of two spine-PAP pairs were analyzed per dendritic segment. For calcium imaging experiments, n represents the number of hippocampal slices where at least eight cells per slice were recorded and averaged. Data are represented as means ± SEM. Statistical tests are indicated in figure legends. Data significance is indicated as follows: n.s. (not significant), *p < 0.05, **p < 0.01, ***p < 0.001, ****p < 0.0001.

Supplemental Information

Supplemental Information includes three figures, Supplemental Experimental Procedures, and three movies and can be found with this article online at http://dx.doi.org/10.1016/j.cub.2014.06.025.

Author Contributions

Y.B. and D.M. conducted in vitro imaging and electrophysiology experiments. Y.B., S.K., and E.V.J. cloned genes into viral vectors. I.N. performed EM measurements. C.E.F. performed immunohistochemistry. E.J. and C.G.B. synthesized FMRFa-NVTEG. J.R. and A.H. performed in vivo experiments. Y.B. generated SFV viruses. K.K.M. contributed to the study design. Y.B. and D.M. designed and supervised the project. Y.B., A.H., and D.M. wrote the manuscript.

Acknowledgments

This work was supported by FP7-IIF-Marie Curie grant 254022 to Y.B. and D.M. and grants from the Swiss National Science Foundation (310030B_144080), NCCR Synapsy, and Novartis Foundation to D.M. We thank L. Jourdain for outstanding technical assistance, J.-Y. Chatton for the LED, X. Dong for Mrg vectors, the BCF of UniGE for Huygens software, and B. Boda for blinded data validation.

Received: April 28, 2014
Revised: June 5, 2014
Accepted: June 10, 2014
Published: July 17, 2014

References

1. Nishida, H., and Okabe, S. (2007). Direct astrocytic contacts regulate local maturation of dendritic spines. J. Neurosci. *27*, 331–340.
2. Volterra, A., and Meldolesi, J. (2005). Astrocytes, from brain glue to communication elements: the revolution continues. Nat. Rev. Neurosci. *6*, 626–640.
3. Ventura, R., and Harris, K.M. (1999). Three-dimensional relationships between hippocampal synapses and astrocytes. J. Neurosci. *19*, 6897–6906.
4. Araque, A., Parpura, V., Sanzgiri, R.P., and Haydon, P.G. (1999). Tripartite synapses: glia, the unacknowledged partner. Trends Neurosci. *22*, 208–215.
5. Porter, J.T., and McCarthy, K.D. (1996). Hippocampal astrocytes in situ respond to glutamate released from synaptic terminals. J. Neurosci. *16*, 5073–5081.
6. Pasti, L., Volterra, A., Pozzan, T., and Carmignoto, G. (1997). Intracellular calcium oscillations in astrocytes: a highly plastic, bidirectional form of communication between neurons and astrocytes in situ. J. Neurosci. *17*, 7817–7830.
7. Hirase, H., Qian, L., Barthó, P., and Buzsáki, G. (2004). Calcium dynamics of cortical astrocytic networks in vivo. PLoS Biol. *2*, E96.
8. Wang, X., Lou, N., Xu, Q., Tian, G.F., Peng, W.G., Han, X., Kang, J., Takano, T., and Nedergaard, M. (2006). Astrocytic Ca2+ signaling evoked by sensory stimulation in vivo. Nat. Neurosci. *9*, 816–823.
9. Fiacco, T.A., and McCarthy, K.D. (2004). Intracellular astrocyte calcium waves in situ increase the frequency of spontaneous AMPA receptor currents in CA1 pyramidal neurons. J. Neurosci. *24*, 722–732.
10. Fellin, T., Pascual, O., Gobbo, S., Pozzan, T., Haydon, P.G., and Carmignoto, G. (2004). Neuronal synchrony mediated by astrocytic glutamate through activation of extrasynaptic NMDA receptors. Neuron *43*, 729–743.
11. Pascual, O., Casper, K.B., Kubera, C., Zhang, J., Revilla-Sanchez, R., Sul, J.Y., Takano, H., Moss, S.J., McCarthy, K., and Haydon, P.G. (2005). Astrocytic purinergic signaling coordinates synaptic networks. Science *310*, 113–116.
12. Jourdain, P., Bergersen, L.H., Bhaukaurally, K., Bezzi, P., Santello, M., Domercq, M., Matute, C., Tonello, F., Gundersen, V., and Volterra, A. (2007). Glutamate exocytosis from astrocytes controls synaptic strength. Nat. Neurosci. *10*, 331–339.
13. Min, R., and Nevian, T. (2012). Astrocyte signaling controls spike timing-dependent depression at neocortical synapses. Nat. Neurosci. *15*, 746–753.
14. Henneberger, C., Papouin, T., Oliet, S.H., and Rusakov, D.A. (2010). Long-term potentiation depends on release of D-serine from astrocytes. Nature *463*, 232–236.
15. Panatier, A., Vallée, J., Haber, M., Murai, K.K., Lacaille, J.C., and Robitaille, R. (2011). Astrocytes are endogenous regulators of basal transmission at central synapses. Cell *146*, 785–798.
16. Di Castro, M.A., Chuquet, J., Liaudet, N., Bhaukaurally, K., Santello, M., Bouvier, D., Tiret, P., and Volterra, A. (2011). Local Ca2+ detection and modulation of synaptic release by astrocytes. Nat. Neurosci. *14*, 1276–1284.
17. Filosa, A., Paixão, S., Honsek, S.D., Carmona, M.A., Becker, L., Feddersen, B., Gaitanos, L., Rudhard, Y., Schoepfer, R., Klopstock, T., et al. (2009). Neuron-glia communication via EphA4/ephrin-A3 modulates LTP through glial glutamate transport. Nat. Neurosci. *12*, 1285–1292.
18. Suzuki, A., Stern, S.A., Bozdagi, O., Huntley, G.W., Walker, R.H., Magistretti, P.J., and Alberini, C.M. (2011). Astrocyte-neuron lactate transport is required for long-term memory formation. Cell *144*, 810–823.
19. Molofsky, A.V., Krencik, R., Ullian, E.M., Tsai, H.H., Deneen, B., Richardson, W.D., Barres, B.A., and Rowitch, D.H. (2012). Astrocytes and disease: a neurodevelopmental perspective. Genes Dev. *26*, 891–907.
20. Chung, W.S., Clarke, L.E., Wang, G.X., Stafford, B.K., Sher, A., Chakraborty, C., Joung, J., Foo, L.C., Thompson, A., Chen, C., et al. (2013). Astrocytes mediate synapse elimination through MEGF10 and MERTK pathways. Nature *504*, 394–400.
21. Haber, M., Zhou, L., and Murai, K.K. (2006). Cooperative astrocyte and dendritic spine dynamics at hippocampal excitatory synapses. J. Neurosci. *26*, 8881–8891.
22. Lavialle, M., Aumann, G., Anlauf, E., Pröls, F., Arpin, M., and Derouiche, A. (2011). Structural plasticity of perisynaptic astrocyte processes involves ezrin and metabotropic glutamate receptors. Proc. Natl. Acad. Sci. USA *108*, 12915–12919.
23. Witcher, M.R., Kirov, S.A., and Harris, K.M. (2007). Plasticity of perisynaptic astroglia during synaptogenesis in the mature rat hippocampus. Glia *55*, 13–23.
24. Lushnikova, I., Skibo, G., Muller, D., and Nikonenko, I. (2009). Synaptic potentiation induces increased glial coverage of excitatory synapses in CA1 hippocampus. Hippocampus *19*, 753–762.
25. Genoud, C., Quairiaux, C., Steiner, P., Hirling, H., Welker, E., and Knott, G.W. (2006). Plasticity of astrocytic coverage and glutamate transporter expression in adult mouse cortex. PLoS Biol. *4*, e343.
26. Caroni, P., Donato, F., and Muller, D. (2012). Structural plasticity upon learning: regulation and functions. Nat. Rev. Neurosci. *13*, 478–490.
27. Ehrengruber, M.U., Renggli, M., Raineteau, O., Hennou, S., Vähä-Koskela, M.J., Hinkkanen, A.E., and Lundstrom, K. (2003). Semliki Forest virus A7(74) transduces hippocampal neurons and glial cells in a temperature-dependent dual manner. J. Neurovirol. *9*, 16–28.
28. Ehrengruber, M.U., Lundstrom, K., Schweitzer, C., Heuss, C., Schlesinger, S., and Gähwiler, B.H. (1999). Recombinant Semliki Forest virus and Sindbis virus efficiently infect neurons in hippocampal slice cultures. Proc. Natl. Acad. Sci. USA *96*, 7041–7046.
29. Shigetomi, E., Bushong, E.A., Haustein, M.D., Tong, X., Jackson-Weaver, O., Kracun, S., Xu, J., Sofroniew, M.V., Ellisman, M.H., and Khakh, B.S. (2013). Imaging calcium microdomains within entire astrocyte territories and endfeet with GCaMPs expressed using adeno-associated viruses. J. Gen. Physiol. *141*, 633–647.

30. Dunaevsky, A., Tashiro, A., Majewska, A., Mason, C., and Yuste, R. (1999). Developmental regulation of spine motility in the mammalian central nervous system. Proc. Natl. Acad. Sci. USA *96*, 13438–13443.
31. De Roo, M., Klauser, P., and Muller, D. (2008). LTP promotes a selective long-term stabilization and clustering of dendritic spines. PLoS Biol. *6*, e219.
32. Mulligan, S.J., and MacVicar, B.A. (2004). Calcium transients in astrocyte endfeet cause cerebrovascular constrictions. Nature *431*, 195–199.
33. Shigetomi, E., Kracun, S., Sofroniew, M.V., and Khakh, B.S. (2010). A genetically targeted optical sensor to monitor calcium signals in astrocyte processes. Nat. Neurosci. *13*, 759–766.
34. Han, S.K., Dong, X., Hwang, J.I., Zylka, M.J., Anderson, D.J., and Simon, M.I. (2002). Orphan G protein-coupled receptors MrgA1 and MrgC11 are distinctively activated by RF-amide-related peptides through the Galpha q/11 pathway. Proc. Natl. Acad. Sci. USA *99*, 14740–14745.
35. Fiacco, T.A., Agulhon, C., Taves, S.R., Petravicz, J., Casper, K.B., Dong, X., Chen, J., and McCarthy, K.D. (2007). Selective stimulation of astrocyte calcium in situ does not affect neuronal excitatory synaptic activity. Neuron *54*, 611–626.
36. Matsuzaki, M., Honkura, N., Ellis-Davies, G.C., and Kasai, H. (2004). Structural basis of long-term potentiation in single dendritic spines. Nature *429*, 761–766.
37. Heo, J., Han, S.K., Vaidehi, N., Wendel, J., Kekenes-Huskey, P., and Goddard, W.A., 3rd. (2007). Prediction of the 3D structure of FMRF-amide neuropeptides bound to the mouse MrgC11 GPCR and experimental validation. ChemBioChem *8*, 1527–1539.
38. Bernardinelli, Y., Haeberli, C., and Chatton, J.Y. (2005). Flash photolysis using a light emitting diode: an efficient, compact, and affordable solution. Cell Calcium *37*, 565–572.
39. Holtmaat, A., Bonhoeffer, T., Chow, D.K., Chuckowree, J., De Paola, V., Hofer, S.B., Hübener, M., Keck, T., Knott, G., Lee, W.C., et al. (2009). Long-term, high-resolution imaging in the mouse neocortex through a chronic cranial window. Nat. Protoc. *4*, 1128–1144.
40. Devaraju, P., Sun, M.Y., Myers, T.L., Lauderdale, K., and Fiacco, T.A. (2013). Astrocytic group I mGluR-dependent potentiation of astrocytic glutamate and potassium uptake. J. Neurophysiol. *109*, 2404–2414.
41. Bezzi, P., Gundersen, V., Galbete, J.L., Seifert, G., Steinhäuser, C., Pilati, E., and Volterra, A. (2004). Astrocytes contain a vesicular compartment that is competent for regulated exocytosis of glutamate. Nat. Neurosci. *7*, 613–620.
42. Bernardinelli, Y., Magistretti, P.J., and Chatton, J.Y. (2004). Astrocytes generate Na+-mediated metabolic waves. Proc. Natl. Acad. Sci. USA *101*, 14937–14942.
43. Paoletti, P., Bellone, C., and Zhou, Q. (2013). NMDA receptor subunit diversity: impact on receptor properties, synaptic plasticity and disease. Nat. Rev. Neurosci. *14*, 383–400.
44. Xu, T., Yu, X., Perlik, A.J., Tobin, W.F., Zweig, J.A., Tennant, K., Jones, T., and Zuo, Y. (2009). Rapid formation and selective stabilization of synapses for enduring motor memories. Nature *462*, 915–919.
45. Yang, G., Pan, F., and Gan, W.B. (2009). Stably maintained dendritic spines are associated with lifelong memories. Nature *462*, 920–924.
46. Anwyl, R. (2009). Metabotropic glutamate receptor-dependent long-term potentiation. Neuropharmacology *56*, 735–740.
47. Boda, B., Mendez, P., Boury-Jamot, B., Magara, F., and Muller, D. (2014). Reversal of activity-mediated spine dynamics and learning impairment in a mouse model of Fragile X syndrome. Eur. J. Neurosci. *39*, 1130–1137.
48. Kucukdereli, H., Allen, N.J., Lee, A.T., Feng, A., Ozlu, M.I., Conatser, L.M., Chakraborty, C., Workman, G., Weaver, M., Sage, E.H., et al. (2011). Control of excitatory CNS synaptogenesis by astrocyte-secreted proteins Hevin and SPARC. Proc. Natl. Acad. Sci. USA *108*, E440–E449.
49. Jones, E.V., Bernardinelli, Y., Tse, Y.C., Chierzi, S., Wong, T.P., and Murai, K.K. (2011). Astrocytes control glutamate receptor levels at developing synapses through SPARC-beta-integrin interactions. J. Neurosci. *31*, 4154–4165.
50. Holtmaat, A.J., Trachtenberg, J.T., Wilbrecht, L., Shepherd, G.M., Zhang, X., Knott, G.W., and Svoboda, K. (2005). Transient and persistent dendritic spines in the neocortex in vivo. Neuron *45*, 279–291.
51. Clarke, L.E., and Barres, B.A. (2013). Emerging roles of astrocytes in neural circuit development. Nat. Rev. Neurosci. *14*, 311–321.
52. Mendez, P., De Roo, M., Poglia, L., Klauser, P., and Muller, D. (2010). N-cadherin mediates plasticity-induced long-term spine stabilization. J. Cell Biol. *189*, 589–600.
53. Murai, K.K., Nguyen, L.N., Irie, F., Yamaguchi, Y., and Pasquale, E.B. (2003). Control of hippocampal dendritic spine morphology through ephrin-A3/EphA4 signaling. Nat. Neurosci. *6*, 153–160.
54. Molotkov, D., Zobova, S., Arcas, J.M., and Khiroug, L. (2013). Calcium-induced outgrowth of astrocytic peripheral processes requires actin binding by Profilin-1. Cell Calcium *53*, 338–348.
55. Bushong, E.A., Martone, M.E., Jones, Y.Z., and Ellisman, M.H. (2002). Protoplasmic astrocytes in CA1 stratum radiatum occupy separate anatomical domains. J. Neurosci. *22*, 183–192.
56. Scemes, E., and Giaume, C. (2006). Astrocyte calcium waves: what they are and what they do. Glia *54*, 716–725.
57. Perea, G., and Araque, A. (2005). Properties of synaptically evoked astrocyte calcium signal reveal synaptic information processing by astrocytes. J. Neurosci. *25*, 2192–2203.
58. Benediktsson, A.M., Schachtele, S.J., Green, S.H., and Dailey, M.E. (2005). Ballistic labeling and dynamic imaging of astrocytes in organotypic hippocampal slice cultures. J. Neurosci. Methods *141*, 41–53.
59. Solomek, T., Mercier, S., Bally, T., and Bochet, C.G. (2012). Photolysis of ortho-nitrobenzylic derivatives: the importance of the leaving group. Photochem. Photobiol. Sci. *11*, 548–555.
60. Bernardinelli, Y., Salmon, C., Jones, E.V., Farmer, W.T., Stellwagen, D., and Murai, K.K. (2011). Astrocytes display complex and localized calcium responses to single-neuron stimulation in the hippocampus. J. Neurosci. *31*, 8905–8919.
61. Dubos, A., Combeau, G., Bernardinelli, Y., Barnier, J.V., Hartley, O., Gaertner, H., Boda, B., and Muller, D. (2012). Alteration of synaptic network dynamics by the intellectual disability protein PAK3. J. Neurosci. *32*, 519–527.